

# Fault-Tolerant Capability and Torque-Speed Measurements of Permanent Magnet Brushless AC Machines



C. C. Awah\*, O. I. Okoro

Department of Electrical and Electronic Engineering, Michael Okpara University of Agriculture, Umudike, Nigeria.



**ABSTRACT:** In this paper, the fault-tolerant capability in terms of inductance profile of a dual-stator permanent magnet brushless AC machine is presented. Similarly, its power-speed and torque-speed characteristics are also predicted. Special reference is made to the impact of different rotor pole numbers. A 2D-finite element analysis (FEA) procedure is adopted in this work, and the cross-coupling effect of the machine inductances owing to the influence of direct-axis and quadrature-axis currents is also taken into consideration. The results show that, the investigated machine having odd number of rotor poles would exhibit better fault-tolerant capability compared to their counterparts with even number of rotor poles. Further, the machine having 6-stator slots and 13-rotor poles *i.e.* 6Slots-13P machine has the greatest field-weakening potential owing to its high full-speed to rated speed relation. The studies also show that, the investigated machines have negligible reluctance torque due to their basically unity saliency ratios obtained from the machines' almost similar quadrature-axis inductance,  $L_q$ , and direct-axis inductance,  $L_d$ , values.

**KEYWORDS:** Direct-axis, Quadrature-axis, Inductance, Power, Speed, Torque, AC machines, Permanent magnet.

[Received February 5, 2019; Revised April 22, 2019; Accepted May 29, 2019]

Print ISSN: 0189-9546 | Online ISSN: 2437-2110

## I. INTRODUCTION

The fault-tolerant potential of any given electric machine is an important parameter to be considered by any good machine designer, especially, for the interest of the machine's reliability. Also, the knowledge about torque-speed and power potentials of a given electrical machine is essential to determine its field-weakening ability in the constant power and constant torque regions of operation. Therefore, the prediction of torque-speed and power-speed characteristics, as well as, the inductance features of a brushless AC permanent magnet machine is given in this study.

The fault-tolerant potential in terms of high self-inductance values of permanent magnet (PM) machines could be improved by increasing the winding layers of the machine. Thus, the higher the winding layer, the larger its self-inductance values as proven in Hwang *et al* (2014) and consequently, the better it's fault-withstand capability. It is reconfirmed in Wu *et al* (2018), that both the overload withstand capacity and the overall torque performance of a machine would be enriched at higher self-inductance value, due to the lower effect of electric and magnetic loadings on electrical machine that has large self-inductance worth. However, an alternative approach to improve the fault-tolerant capability and hence, the reliability of PM machines is by adopting multi-phase systems as detailed in Xue *et al* (2013) and Li *et al* (2015). Note that, this method of using multi-phase system is also good for the flexibility of electric machine control techniques. In addition, the use of modular structure to isolate the possible phase mutual-couplings in the

windings as detailed in Ede *et al* (2007) and Atallah *et al* (2003) could also enhance the fault-tolerance ability of PM machines; also with a resultant higher amount of self-inductance Zhao *et al* (2017), relative to conventional non-modular PM machines.

The torque-speed and power-speed characteristics of switched-flux permanent magnet machines are explored in Hua *et al* (2006), with special reference to the sizing equations in relation to the inverter capability. The studies in Hua *et al* (2006) found that the field-weakening region of PM machine could be enhanced by increasing either the current density and, or the slot fill factor of the machine, if possible. Similarly, it is stated in Fei *et al* (2012) that the constant-power speed range of a switched flux PM machine could be improved by either increasing its direct-axis inductance or by reducing the permanent magnet flux linkage of the machine. This is achieved by segmenting small portions of the PMs with iron bridges, in order to provide magnetic saturation on the machine Fei *et al* (2012). Further in support of the obtained results in Fei *et al* (2012), the segmentation of permanent magnets by iron bridges in interior permanent magnet machines is proven to be effective in enhancing the field-weakening capability of the machine through the created flux-leakage paths of the irons, as investigated in Duan *et al* (2014).

Alternatively, it is preferable to optimize a machine such that the magnitude of its quadrature-axis inductance is larger than the corresponding direct-axis inductance during the design / optimization stage. Moreover, the field-weakening

\*Corresponding author: ccawah@iee.org

potential of a brushless PM machine with corresponding broader operating speed range could be achieved by introducing a double-layered PM per pole topology, as presented in Zhu *et al* (2016). This is contrary to the traditional single PM per pole arrangement obtainable in the conventional interior permanent magnet synchronous machine. More so, the field-weakening potential of switched flux PM machine could be improved by the use of suitable lamination style *i.e.* the laminations stacked in parallel with shaft axis yields better results than that of the conventional axially-laminated method of the core materials being laminated in the direction of the shaft axis (Xu *et al*, 2012).

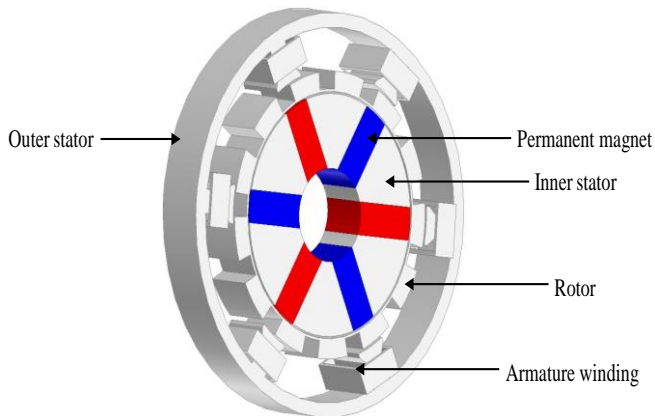


Figure 1: Structural View of the Developed Three-Phase AC Machine.

Different field-weakening control strategies for effective extension of the constant-power speed operation in drive applications, such as the adjustment of the axial gap between the stator and rotor parts (Kim, 2012), and production of sinusoidal electromotive force (EMF) waveforms (Chaithongsuk *et al*, 2012), as well as control of the machine's current advance angle etc. are readily available in literature.

Furthermore, a comparative study on rotor-positioned permanent magnet (RPPM) and stator-positioned permanent magnet (SPPM) machines given in Su *et al* (2019) shows that the RPPM machine has better field weakening capability than its equivalent SPPM machine under the same current condition, due to the small amount of flux-linkage contributed by the armature reaction in the SPPM machine.

The possible stator pole,  $P_s$  and rotor pole,  $P_r$  combination of the compared machines is given in (1).

$$2P_s \pm n = P_r \quad (1)$$

where  $n$  is a positive integer (Awah, 2016).

The developed machine model shown in Figure 1 is different from that with  $P_s \pm n = P_r$  presented in Evans and Zhu (2015). It should be noted that, the PM volume of the developed machine in this study is over 22% smaller than the one presented in Evans and Zhu (2015). Thus, the developed machine in Evans and Zhu (2015) would be more expensive than the one presented in this study. Note also, that the compared machine in this study is equivalent to that given in Chen and Zhu (2010); however, the investigated machine is a

dual-stator PM machine while the structure in Chen and Zhu (2010) is a single-stator machine topology. In addition, the permanent magnets (PMs) are separated from the windings and relocated to the inner segmented stator in this present study, while the PMs are positioned together with the windings in the former study. Moreover, the developed model in this present study could enhance the demagnetization-withstand capability of the machine, since the effect of armature reaction from the conductors is greatly reduced.

Furthermore, the magnetic vector field of the investigated machine, on no-load condition, is displayed in Figure 2. It is obvious that, there could be some leakage flux from the outer-stator yoke of the machine. Therefore, it is necessary to provide a magnetic field-shield on the back-iron to reduce the impact of leakage flux on the machine during its operation.

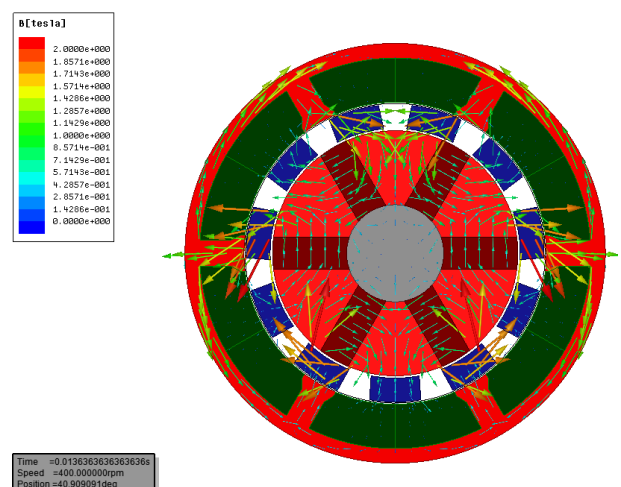


Figure 2: Magnetic Vector Fields of the Developed Machine at No-Load.

Zhou *et al* (2018), showed that the saliency ratio of a given permanent magnet machine is slightly dependent on its direct-axis current, and highly reliant on the quadrature-axis current. However, Zhu *et al* (2016) noted that the level of disparity between the magnitudes of direct-axis and quadrature-axis inductances would be determined by the current angle of the machine. Zhou *et al* (2018) further stated that, the overall output torque of a given electric machine is influenced by the value of its direct-axis and quadrature-axis currents. It should also be noted that, the quadrature-axis current of a machine is inversely related to its saliency ratio, due to saturation effect. Similarly, the studies in He *et al* (2018), presented that the value of winding inductance of PM machine is adversely reduced at higher input currents, owing to the attendant core saturation problems.

It is worth noting that, the investigated machine combines the advantages of switched-flux PM machines and those of magnetically-g geared PM machines in one integrated system. Day by day, magnetically-g geared machines are becoming an interesting research area due to their enormous benefits which includes: high efficiency, large output torque and high power capability compared to other permanent magnet machines of the same size as pointed out in Tlali *et al* (2016) and Zhang *et al* (2016).

According to Atallah *et al* (2004), the general expression for the angular velocity of the dual rotor-PMs in a given magnetic gear machine having two rotating parts and a stationary steel piece is given in (2). It should be noted that, the stationary steel piece which serves as the modulator in Atallah *et al* (2004) is equivalent to the rotating modulating ring *i.e.* the cup-rotor in this present paper.

$$\omega_{i,j} = \frac{ip}{ip + jn_s} \omega_r + \frac{jn_s}{ip + jn_s} \omega_s \quad (2)$$

where  $\omega_r$  and  $\omega_s$  are the rotational velocities. The maximum torque transmission is obtained at  $i=1$  and  $j=-1$  as stated in Atallah *et al* (2004) and cited in (Awah, 2016).

When the outer rotor magnets are interchanged with the outer-stator conductors having the cup-rotor in operation; then, the gear ratio of the developed machine in this paper is given in eqn (3).

$$G_{ratio} = \frac{-1 * (j) * P_s}{iP_r} = \frac{P_s}{P_r} \quad (3)$$

## II. METHODOLOGY

The first step is the transformation of the  $I_d$  and  $I_q$  currents into  $ABC$  currents. For example, the FEA inputted currents are expressed using eqn (4). Note that, the zero-sequence component is neglected in this analysis because we assumed a balanced three-phase system with injected purely sinusoidal current components. The inductance prediction approach of using the flux-linkages as detailed in Qi *et al* (2009) and expressed in eqns (5) and (6) is employed in the prediction of the machines' direct-axis and quadrature-axis inductances. This is obtained by the use of the traditional Park's transformation scheme.

$$\begin{bmatrix} I_d \\ I_q \end{bmatrix} = \frac{2}{3} \begin{bmatrix} \cos\theta & \cos(\theta - 120^\circ) & \cos(\theta + 120^\circ) \\ -\sin\theta & -\sin(\theta - 120^\circ) & -\sin(\theta + 120^\circ) \end{bmatrix} \begin{bmatrix} I_A \\ I_B \\ I_C \end{bmatrix} \quad (4)$$

where  $\theta$  is the rotor angular displacement (Zhu *et al*, 2005).

The direct-axis and quadrature-axis inductance of the investigated machine is given in (5) and (6).

$$L_d(I_d) = \frac{\varphi_d(I_d = I_d, I_q = 0) - \varphi_d(I_d = I_q = 0)}{I_d} \quad (5)$$

$$L_q(I_q) = \frac{\varphi_q(I_q = I_q, I_d = 0) - \varphi_q(I_d = I_q = 0)}{I_q} \quad (6)$$

where  $L_d$ ,  $L_q$ , are the direct and quadrature axis inductances, and  $\varphi_d$  and  $\varphi_q$  are the direct and quadrature flux-linkages, respectively (Qi *et al*, 2009).

Note that, the direct-axis and quadrature-axis flux-linkages are obtained from phase A, B, and C flux-linkages using inverse Park's transformation of eqn (4), and simulated over different electrical rotor positions of the FEA model

shown in Figure 1, although with varying number of rotor poles. It must be noted that, the non-linearity with respect to the influence of cross-coupling between the direct- and quadrature axis inductance is taken into cognizance in the inductance predictions, owing to the symbiotic effects of the injected direct-axis and quadrature-axis currents on the machines' winding inductances.

It is worth mentioning that, the predicted torque-speed and power-speed curves are obtained using the average values of the direct-axis and quadrature-axis inductances taken over twenty (20) steps per each of the injected current ( $I_d$  and  $I_q$ ) value. Furthermore, the post-processing of the obtained torque-speed and power-speed curves are completed with the help of MATLAB program / scripts taking into account the  $L_d$  and  $L_q$  inductance matrices, the machine's number of phases, number of poles, voltage and current limitations, slot area and packing factor, rated speed, axial length of the machine, per phase number of turns, and other parameters of eqn (10), etc., as well as the values of the permanent magnet  $d$ -axis flux linkages at different current (Amperes) level. For example, the FEA predicted values of  $L_q$ ,  $L_d$  (Henries) and permanent magnet  $d$ -axis flux linkages (Webers) in plotting of torque-speed and power-speed curves of the 6Slots-11P machine topology are given in Table 1, Table 2 and Table 3, respectively.

It is worth noting that, the values of the permanent magnet flux linkage decreases as the value of the quadrature-axis current rises, due to the influence of armature reaction which would eventually lead to magnetic saturation of the machine at higher input current condition. Also, note that the FEA software automatically generates the phase A, B, and C flux-linkage as well as the induced electromotive force (EMF) results after the time-stepped computation at different rotor angular displacements. Nevertheless, the FEA computations applied in eqns (7) and (8) are conducted under two different conditions: no-load (open-circuit) and full-load current situations, before the post-processing of the results.

$$L_{self} = \frac{\varphi_A - \varphi_{A\_mag}}{I_A} \quad (7)$$

$$L_{Mutual} = \frac{\varphi_B - \varphi_{A\_mag}}{I_B} \quad (8)$$

where  $L_{self}$  and  $L_{mutual}$  are the self and mutual inductance quantities;  $\varphi_A$  and  $\varphi_B$  are the flux-linkages due to the excitation of phase A and phase B windings, respectively;  $I_A$  and  $I_B$  are the phase A and phase B current magnitudes *i.e.* the supplied root mean square current (r.m.s current), respectively, and  $\varphi_{A\_mag}$  is the open-circuit flux linkage of phase A. Note that,  $I_A=I_B$  in magnitude.

Although, the investigated PM machine is an alternating current machine, it is worth noting that r.m.s current is used in the computation of the inductances in eqns (7) and (8). Moreover, the materials and data of the analyzed FEA model of Figure 1 are given in Table 4.

**Table 1: Average quadrature-axis inductances,  $L_q$ .**

Current ( $I_q, I_d$ )	0	-1	-3	-6	-9	-12	-15
1	0.00039677	0.0004019	0.000408533	0.000415202	0.000422237	0.000428966	
3	0.000396122	0.00040083	0.000407954	0.000415122	0.000421894	0.000428027	
6	0.000395904	0.00040077	0.000407728	0.000414474	0.000421002	0.000427208	
9	0.000396702	0.0004013	0.000408032	0.000414645	0.000421091	0.000427153	
12	0.000397193	0.000401777	0.00040847	0.000414942	0.000421062	0.00042678	
15	0.000397547	0.000402181	0.000408737	0.000414888	0.000420693	0.000426239	

**Table 2: Average direct-axis inductances,  $L_d$ .**

Current ( $I_d, I_q$ )	0	1	3	6	9	12	15
-15	0.00044	0.000437815	0.000437553	0.000436855	0.000435805	0.000434425	
-12	0.00043	0.000428985	0.000428696	0.000428181	0.00042731	0.000425899	
-9	0.00042	0.000419617	0.000419307	0.0004188	0.000418164	0.000416628	
-6	0.00041	0.000409551	0.000409316	0.000408518	0.000408069	0.00040643	
-3	0.0004	0.000398431	0.000398508	0.000397134	0.000396716	0.00039513	
-1	0.00039	0.00039004	0.000390763	0.000388818	0.000388279	0.00038711	

**Table 3: Permanent magnet  $d$ -axis flux.**

Current, $I_q$ (A)	D-axis magnet flux-linkage (Wb)
0	0.011517781
3	0.011506036
6	0.011475139
9	0.011420174
12	0.011345361
15	0.011250833

**Table 4: Materials and Data of the analyzed FEA Model.**

Parameter	Data
No. of phases	3
Speed	400rpm
Overall stator diameter	90mm
Back-iron thickness	3.15mm
PM width	4mm
Air-gap length	0.5mm
Machine stack length	25mm
Machine aspect ratio	0.71
PM residual flux density	1.2Tesla
PM material (neodymium-iron-boron)	N38SH
Stator and rotor core material	Silicon steel
Relative permeability	1.05
No. of turns per phase	72

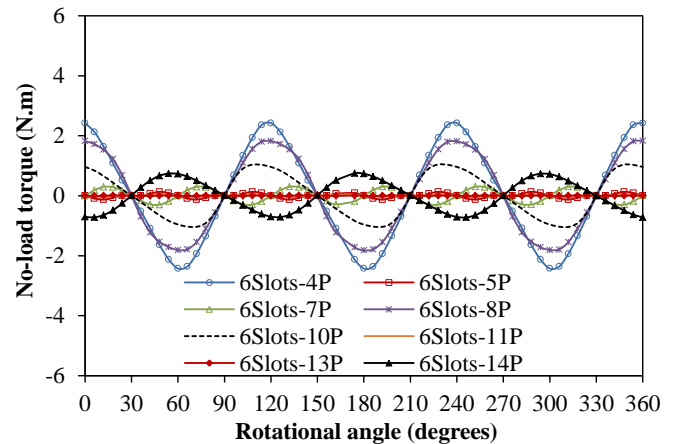
III. STATIC CHARACTERISTICS

Figure 3 shows the torque on no-load condition, and its corresponding Fast Fourier Transform (FFT) amplitudes. The result shows that 3<sup>rd</sup> FFT amplitude is larger in the machine model having even rotor-pole number. As noted in Zhu and Howe (2000), the no-load torque goodness factor,  $T_{nl}$ , of the compared machines is related to the machine’s stator pole and rotor pole number as given in (9). Therefore, if the goodness factor is small, then, the resultant magnitude of the no-load torque would be small. This implies that the overall electromagnetic torque of the machine would be improved, since no-load torque is an undesirable quantity which adversely affects the output torque of a given electric machine. More so, the investigation in Zhu and Howe (2000) shows that PM machines with non-overlapping windings are preferred choice under this situation compared to their overlapping winding counterparts. Moreover, the accuracy of

the no-load torque prediction is largely dependent on the mesh-discretisation level of the designed model as stated in Howe and Zhu (1992). The finer the mesh, the higher the level of accuracy obtained; however, this will entail longer calculation time.

$$T_{nl} = \frac{P_r P_s}{Lcm(P_r, P_s)} \tag{9}$$

where  $P_r$  and  $P_s$  are the rotor and stator pole numbers, and  $Lcm$  is lowest common multiple between the poles (Zhu and Howe, 2000).



(a) Plots

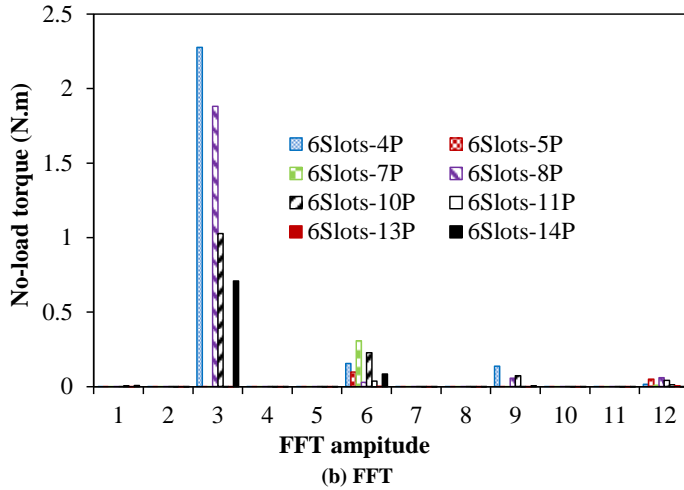


Figure 3: Variation of No-Load Torque.

IV. INDUCTANCE CHARACTERISTICS

The direct-axis inductance and quadrature-axis inductance, in addition to the self-and mutual-inductances of the compared machines are presented in Figures 4 and 5. The inductance profile shows that the compared machine having different rotor poles have relatively similar values of quadrature-axis inductance and direct-axis inductance. Note that, the largest value of quadrature-axis inductance is seen in the 6Slots-5P machine topology.

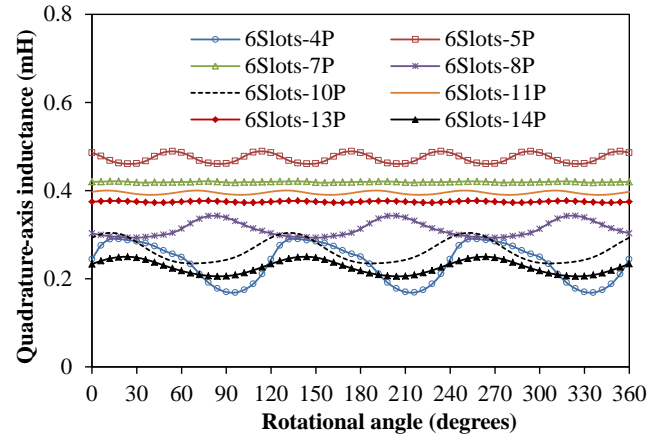
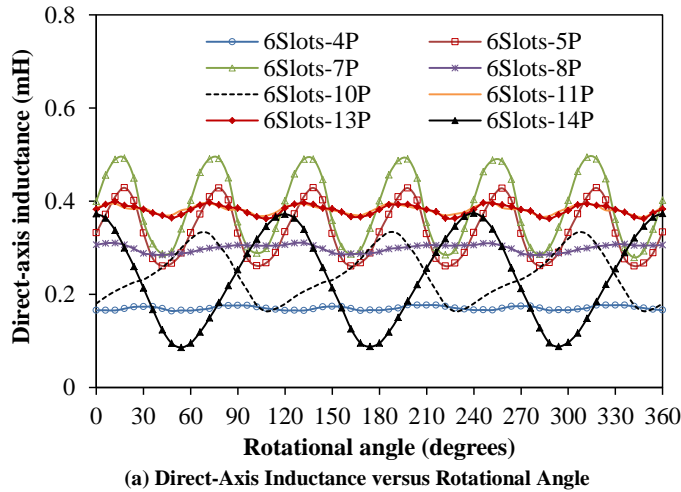
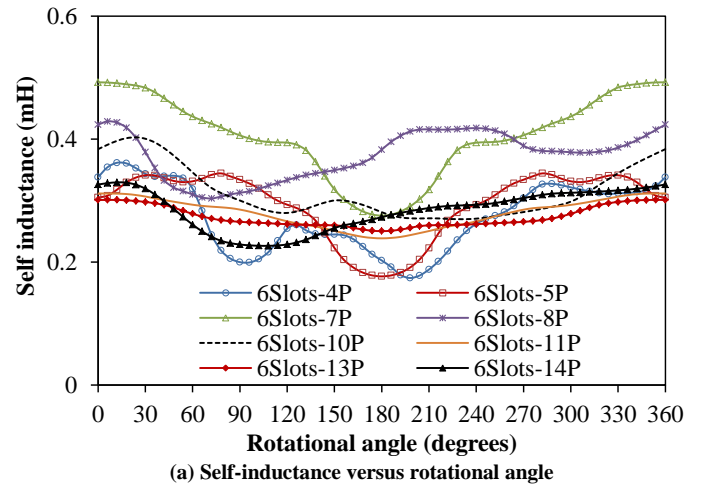


Figure 4: Comparison of Machine D- and Q-axis Inductances.

Similarly, the self-inductance and mutual-inductance waveforms of the analyzed machine relative to different rotor positions are compared in Figure 5(a) and (b), respectively, and expressed in eqns (7) and (8).

It is observed that, the investigated machines have relatively similar self-inductance values. The machine having odd rotor pole numbers have better potentials in terms of higher reliability than the ones having even rotor pole numbers, owing to their low mutual inductance magnitudes. However, the mutual inductance of an integrated PM machine could be significantly reduced to a negligible value by an appropriate winding design and reasonable stator and rotor pole selections, as established in Ren *et al* (2019).

This concept of mutual-inductance reduction is further confirmed by analytical method of employing the winding function technique, in addition to adequate experimental validation. It is worth mentioning that, a small ratio of mutual inductance to self-inductance value is required to improve the reliability of electric machines, as proven in Zhu *et al* (2017). The predicted winding inductance values of the compared machine are listed in Table 5.



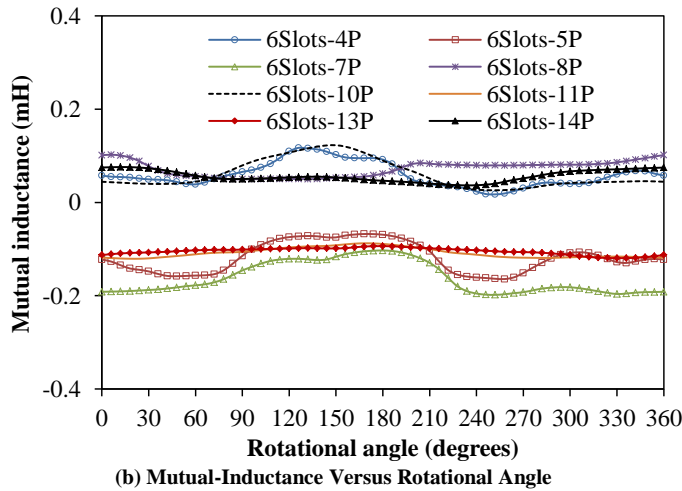


Figure 5: Comparison of the Machine Winding Inductances,  $I_A=15$ Amperes.

## V. TORQUE-SPEED AND POWER-SPEED CHARACTERISTICS

The field-weakening characteristics of the compared machine are depicted in Figure 6. It is worth noting, that the best and poorest electromagnetic torque performance is obtained in the 6Slots-11P and 6Slots-8P machines, respectively. The best candidate amongst the compared machines in terms of field-weakening proficiency is the 6Slots-13P due to its high full speed-to-rated speed proportion. It should be noted that, the effect of cross-coupling on the inductances as detailed in Qi *et al* (2009) is taken into cognizance in the FEA estimation of the torque and power plots of Figure 6. The field-weakening potentials of the analyzed machine are listed in Table 5. Note that, the output power of the compared machine is given in (10).

$$P_{out} = \eta \frac{N_{ph}}{T} \int_0^T e(t)i(t)dt \quad (10)$$

where  $e(t)$  and  $i(t)$  are the time-varying induced EMF and current values,  $\eta$  is the efficiency,  $N_{ph}$  is the number of phases and  $T$  is the period.

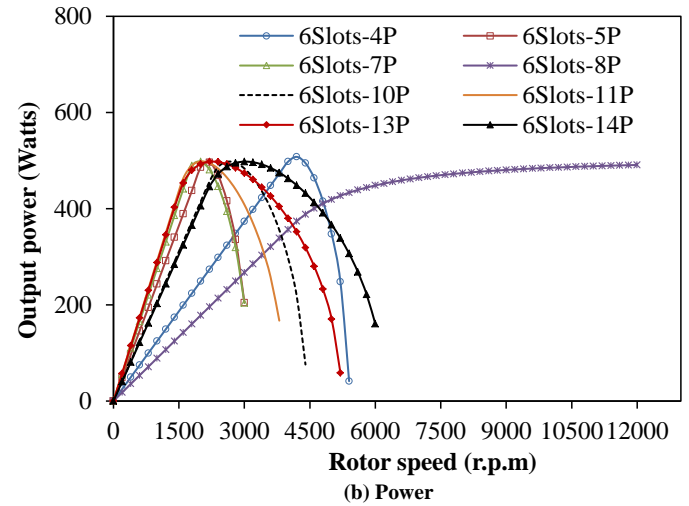
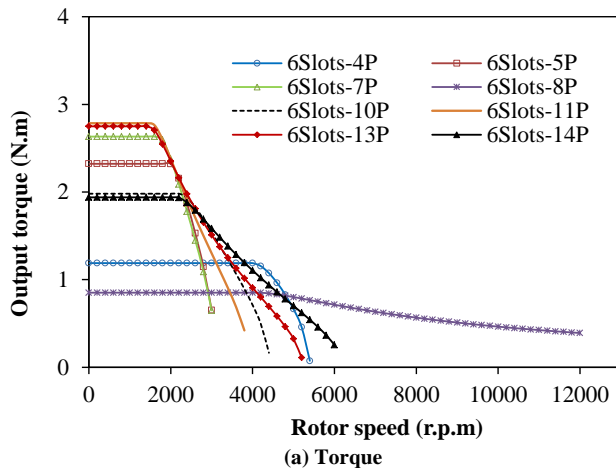


Figure 6: Comparison of Torque-Speed and Power-Speed.

## VI. CONCLUSION

The inductance and flux-weakening potentials of a dual-stator permanent magnet machine is presented and compared. The results show that the compared machine having 6Slots-13P configuration has the largest field-weakening potential over the entire constant power- and constant torque-speed regions. Moreover, the investigated machine having different rotor pole numbers have comparable constant power values as well as negligible reluctance torque. Further, the investigated machine having odd number of rotor poles possess higher fault-tolerant potentials than their even rotor pole number equivalents. Above all, the studied machine topology equipped with eight (8) number of rotor poles has the worst overall performance.

## REFERENCES

- Atallah, K.; J. Wang and D. Howe. (2003). Torque-ripple minimization in modular permanent-magnet brushless machines. *IEEE Transactions on Industry Applications*, 39(6): 1689-1695.
- Atallah, K.; S. D. Calverley and D. Howe. (2004). Design, analysis and realisation of a high performance magnetic gear. *IEE Proceedings-Electric Power Applications*, 151 (2): 135-143.
- Awah, C. C. (2016). Novel double stator switched flux permanent magnet machines. Unpublished PhD Thesis, Department of Electronic and Electrical Engineering, University of Sheffield, UK.
- Chaithongsuk, S.; B. N. Mobarakeh, J. P. Caron, N. Takorabet and F. M. Tabar. (2012). Optimal design of permanent magnet motors to improve field-weakening performances in variable speed drives. *IEEE Transactions on Industrial Electronics*, 59(6): 2484-2494.
- Chen, J.T. and Zhu, Z.Q. (2010). Winding configurations and optimal stator and rotor pole combination of flux switching PM brushless AC machines. *IEEE Transactions on Energy Conversion*, 25(2): 293-302.

**Table 5: Analyzed Machine Values.**

Element	Quantity							
	6S-4P	6S-5P	6S-7P	6S-8P	6S-10P	6S-11P	6S-13P	6S-14P
<b>Machine type</b>								
Direct-axis inductance ( mH)	0.218	0.475	0.479	0.325	0.268	0.434	0.431	0.251
Quadrature-axis inductance (mH)	0.265	0.538	0.459	0.3105	0.279	0.426	0.401	0.235
Saliency ratio	1.2	1.1	0.96	0.96	1.03	0.98	0.93	0.94
Magnet flux (milli Webers)	13.17	20.5	16.71	4.73	8.79	11.251	9.396	6.155
Rated speed (r.p.m)	3900	2000	1700	4000	2200	1500	1400	2100
Full speed (r.p.m)	5400	3100	3100	12000	4500	4000	5300	6300
Full speed / rated speed	1.38	1.55	1.82	3	2.05	2.67	3.79	3
Output torque (N.m)	1.19	2.32	2.63	0.85	1.98	2.785	2.75	1.94
Output power (Watts)	507.87	507.19	507.60	490.99	506.96	507.23	507.12	506.93
Self-inductance (milli Henry)	0.274	0.295	0.406	0.374	0.314	0.280	0.274	0.285
Mutual inductance (milli Henry)	0.059	-0.118	-0.162	0.072	0.0599	-0.108	-0.105	0.057
Mutual inductance/Self inductance	0.215	-0.4	-0.39	0.193	0.191	-0.386	-0.383	0.2
Power factor	0.73	0.75	0.4	0.44	0.82	0.63	0.6	0.9

Note: 6S-4P represents 6-stator slots and 4-rotor poles, etc.

**Duan, S.; L. Zhou and J. Wang. (2014).** Flux weakening mechanism of interior permanent magnet synchronous machines with segmented permanent magnets. *IEEE Transactions Applied on Superconductivity*, 24(3): 0500105.

**Ede, J. D.; K. Atallah, G. W. Jewell, J. B. Wang and D. Howe. (2007).** Effect of axial segmentation of permanent magnets on rotor loss in modular permanent-magnet brushless machines. *IEEE Transactions on Industry Applications*, 43 (5): 1207-1213.

**Evans, D. J. and Zhu, Z. Q. (2015).** Novel partitioned stator switched flux permanent magnet machines. *IEEE Transactions on Magnetics*, 51(1): 8100114.

**Fei, W.; P. C. K. Luk, J. X. Shen, Y. Wang and M. Jin. (2012).** A novel permanent-magnet flux switching machine with an outer-rotor configuration for in-wheel light traction applications, *IEEE Transactions on Industry Applications*, 48(5): 1496-1506.

**He, M.; W. Xu, C. Ye and W. Hua. (2018).** Design of hybrid excited asymmetric-stator-pole doubly salient machine. Paper presented at IEEE International Conference on Electrical Machines (ICEM2018), Alexandroupoli, Greece, 2105-2111.

**Howe, D. and Zhu, Z. Q. (1992).** The influence of finite element discretisation on the prediction of cogging torque in permanent magnet excited motors. *IEEE Transactions on Magnetics*, 28(2), 1080-1083.

**Hua, W.; M. Cheng, Z. Q. Zhu and H. David. (2006).** Design of flux-switching permanent magnet machine considering the limitation of inverter and flux-weakening capability. In *proc. IEEE Industry Applications Annual Conference Meeting, Tampa, FL*, 2403-2410.

**Hwang, C. C.; C. M. Chang, S. S. Hung and C. T. Liu. (2014).** Design of high performance flux switching PM machines with concentrated windings. *IEEE Transactions on Magnetics*, 50(1): 4002404.

**Kim, K. C. (2012).** A novel magnetic flux weakening method of permanent magnet synchronous motor for electric vehicles. *IEEE Transactions on Magnetics*, 48(11): 4042-4045.

**Li, F.; W. Hua, M. Tong, G. Zhao and M. Cheng. (2015).** Nine-phase flux-switching permanent magnet brushless machine for low-speed and high-torque applications. *IEEE Transactions on Magnetics*, 51(3): 8700204.

**Qi, G.; J. T. Chen, Z. Q. Zhu, D. Howe, L. B. Zhou and C. L. Gu. (2009).** Influence of skew and cross-coupling on d- and q-axis inductances and flux-weakening performance of PM brushless AC machines. *IEEE Transactions on Magnetics*, 45(5): 2110-2117.

**Ren, X.; D. Li, R. Qu, W. Kong, X. Han and T. Pei. (2019).** Analysis of spoke-type brushless dual-electrical-port dual-mechanical-port machine with decoupled windings. *IEEE Transactions on Industrial Electronics*, 66(8): 6128-6140.

**Su, P.; W. Hua, Z. Wu, Z. Chen, G. Zhang and M. Cheng. (2019).** Comprehensive comparison of rotor permanent magnet and stator permanent magnet flux-switching machines. *IEEE Transactions on Industrial Electronics*, 66(8): 5862-5871.

**Tlali, P. M.; S. Gerber and R. J. Wang. (2016).** Optimal design of an outer-stator magnetically geared permanent magnet machine. *IEEE Transactions on Magnetics*, 52(2): 8100610.

**Wu, M.; W. Zhao, J. Ji, J. Zheng and J. Luo. (2018).** Reduction of tooth harmonic in fractional-slot concentrated-winding permanent-magnet machines using new stator design. *Journal of Magnetics*, 23(2): 218-228.

**Xu, W.; G. Lei, T. Wang, X. Yu, J. Zhu and Y. Guo. (2012).** Theoretical research on new laminated structure flux switching permanent magnet machine for novel topologic plug-in hybrid electrical vehicle. *IEEE Transactions on Magnetics*, 48(11): 4050-4053.

**Xue, X.; W. Zhao, J. Zhu, G. Liu, X. Zhu and M. Cheng. (2013).** Design of five-phase modular flux-switching permanent-magnet machines for high reliability applications. *IEEE Transactions on Magnetics*, 49(7): 3941-3944.

**Zhang, X.; X. Liu and Z. Chen. (2016).** A novel coaxial magnetic gear and its integration with permanent-magnet brushless motor. *IEEE Transactions Magnetics*, 52(7): 8203304.

**Zhao, J.; Y. Zheng, C. Zhu, X. Liu and B. Li. (2017).** A novel modular-stator outer-rotor flux-switching permanent-magnet motor. *Energies*, 10(7): 937-956.

**Zhou, C.; X. Huang, Y. Fang and L. Wu. (2018).** Comparison of PMSMs with different rotor structures for EV application. Paper presented at IEEE International Conference on Electrical Machines (ICEM2018), Alexandroupoli, Greece, 609-614, USA: IEEE.

**Zhu, X.; S. Yang, Y. Du, Z. Xiang and L. Xu. (2016).** Electromagnetic performance analysis and verification of a new flux-intensifying permanent magnet brushless motor with two-layer segmented permanent magnets. *IEEE Transaction on Magnetics*, 52(7): 8204004.

**Zhu, X.; W. Zhao, J. Zhu and F. Bian. (2017).** A high power factor fault-tolerant vernier permanent-magnet machine. *American Institute of Physics Advances*, 7(5): 056622.

**Zhu, Z. Q. and Howe, D. (2000).** Influence of design parameters on cogging torque in permanent magnet machines. *IEEE Transactions on Magnetics*, 15(4): 407-412.

**Zhu, Z. Q.; Y. Pang, D. Howe, S. Iwasaki, R. Deodhar and A. Pride. (2005).** Analysis of electromagnetic performance of switched flux switching permanent magnet machines by non-linear adaptive lumped parameter magnetic circuit model. *IEEE Transactions on Magnetics*, 41(11): 4277-4287.